Atmospheric Environment 59 (2012) 30–38

Contents lists available at SciVerse ScienceDirect

Atmospheric Environment

journal homepage: www.elsevier.com/locate/atmosenv

Statistical analysis of 4-year observations of aerosol sizes in a semi-rural continental environment

Vijay P. Kanawade [1], David R. Benson [2], Shan-Hu Lee*

College of Public Health, Kent State University, Kent, OH, USA

HIGHLIGHTS

- We provide long-term observations of new particle formation in a semi-rural continental environment of the U.S.
- Seasonal frequency of new particle formation is higher in the spring and fall than in summer and winter.
- Nucleation and growth rates show different seasonal variations.
- The frequent occurrence of new particle formation is related to the transported air masses from polluted power plants.

ARTICLE INFO

Article history:
Received 14 February 2012
Received in revised form
21 May 2012
Accepted 22 May 2012

Keywords:
Ultrafine particles
Particle size distribution
Nucleation
Growth
Air mass history

ABSTRACT

We have made long-term observations of particle size distributions in a semi-rural continental environment of the United States (Kent, Ohio) over a 4-year period, to investigate the seasonal trend of new particle formation (NPF). NPF events occurred throughout the year, but more frequently during the spring (~40%) and fall (~32%) than in the summer (~19%) and winter (~17%). The particle nucleation rates were also highest in the spring (with the median and standard deviation value of $6.8 \pm 1.3\ cm^{-3}\ s^{-1}$) and lowest in the winter ($1.0 \pm 0.9\ cm^{-3}\ s^{-1}$). Particle growth rates were highest in the summer ($6.4 \pm 0.4\ nm\ h^{-1}$) and lowest in the winter ($4.2 \pm 0.3\ nm\ h^{-1}$), a trend different from nucleation rates, indicating that different chemical species may be involved in particle nucleation and growth processes. Backward trajectory calculations show that NPF events were often associated with air masses originated from the east–southeast where numerous large size power plants are located, containing high sulfur dioxide (SO_2). The NPF events in general had lower relative humidity, lower surface area of pre-existing particles, and higher solar radiation.

1. Introduction

Formation of new aerosol particles via gas-to-particle conversion is an important process, which determines the atmospheric aerosol number concentrations. Considerable efforts have been devoted to understanding how new particle formation (NPF) processes lead to formation of cloud condensation nuclei (CCN). Modeling studies suggested that NPF can contribute nearly 15–55% of the global CCN production (Spracklen et al., 2008). A recent observation made at a remote-forested site showed that newly formed particles grew rapidly with a 10–25% probability to CCN sizes (~200 nm) over few days (Pierce et al., 2012).

Field studies have shown that NPF is strongly correlated with a gas phase sulfuric acid (H_2SO_4) (Erupe et al., 2010; Kuang et al., 2008) and low surface area of pre-existing particles (Clarke, 1992). Other chemical species can be also involved in particle nucleation, including ammonia (Weber et al., 1999), organic compounds (Marti et al., 1997) and ions (Lee et al., 2003; Lovejoy et al., 2004). A chemical analysis of nanoparticles in the urban Mexico City also showed that ultrafine particles contained organics, sulfate, and nitrate (Smith et al., 2008). Numerous observations (Sihto et al., 2006 and references therein) including our previous observation in Kent, Ohio (Erupe et al., 2010) also showed that H_2SO_4 alone could explain only 10–30% of the total observed growth, indicating additional chemical species are required to explain the total growth of newly formed particles.

NPF has been reported in a variety of locations (Kulmala et al., 2004 and references therein), but long-term observations of particle size distributions are relatively sparse. Long-term observations were previously made in urban (Stanier et al., 2004a; Wehner and Wiedensohler, 2003), rural-remote (Kivekaas et al.,

* Corresponding author.
E-mail address: slee19@kent.edu (S.-H. Lee).
[1] Present address: Department of Civil Engineering, Indian Institute of Technology, Kanpur, India
[2] Present address: University of Mount Union, Department of Chemistry, Alliance, OH, USA

1352-2310/$ – see front matter © 2012 Elsevier Ltd. All rights reserved.
http://dx.doi.org/10.1016/j.atmosenv.2012.05.047

Table 1
A summary of particle number concentrations at various locations based on long-term measurements.

Location	Site	Measurement period	Size range (nm)	Conc. (cm^{-3})	References
Pittsburgh, PA	Urban	Jul 2001–Jun 2002	3–500	22,000	(Stanier et al., 2004a)
Leipzig, Germany	Urban	Feb 1997–Feb 2001	3–800	21,377	(Wehner and Wiedensohler, 2003)
Waligun, China	Rural-remote	Sep 2005–May 2007	12–570	2030	(Kivekaas et al., 2009)
Hyytiälä, Finland	Rural-pine forest	1999–2001	3–500	2100	(Laakso et al., 2003)
Kent, OH	Semi-rural	2006–2009	3–600	6865	This study

2009), rural boreal forest (Laakso et al., 2003) (Table 1), mixed coniferous and deciduous forest (Tunved et al., 2003), and the high altitude free troposphere (Hallar et al., 2011). These measurements showed that NPF can be related to several factors, including primary emissions by automobiles (e.g. traffic) and stationary (e.g. power plant) sources (Morawska et al., 2002), meteorological conditions (Stanier et al., 2004b), and long-range transport (Kulmala et al., 2000).

Here, we present statistical analysis of long-term observations of particle size distribution made in a semi-rural continental environment (Kent, Ohio). Particle size distributions in the diameter range from 3 to 1000 nm were measured over a 4-year period (2006–2009). NPF studies have been conducted typically in polluted urban areas in the United States, such as Pittsburgh (Stanier et al., 2004b) and Atlanta (McMurry et al., 2005), but long-term measurements of NPF in the less polluted environments are rare in northern America, and to our knowledge there has been only one report of two-year observations in Indiana (Pryor et al., 2010). Previously, we have analyzed the correlation of nucleation rates with H_2SO_4 and ammonia from a year of measurements at this site (Erupe et al., 2010), but the present study focuses on the statistical analysis of long-term measurements of aerosol size distribution. We have used the NPF term in the present study to be consistent with the terminology used in the current literature, but since our measured aerosol sizes can show growth of particles larger than 3 nm (as opposed to freshly nucleated sub-3 nm particles and clusters which were not measured), in practice, NPF implies "growth of new particles".

2. Methods

2.1. Sampling site

Fig. 1 shows the location of the sampling site, Kent (41.15°N, 81.36°W) on the regional map. Kent has a population of about 28,000 and is surrounded by several urban areas, Akron about 30 km to the southwest, Cleveland about 65 km to the northwest, Columbus about 220 km to the southwest, and Pittsburgh about 160 km to the east. Kent may be identified as a semi-rural environment, based on various air pollutants (Ozone, SO_2, NO_x and particulate matter less than 2.5 μm, $PM_{2.5}$) reported by the U.S. Environmental Protection Agency (http://www.epa.gov/air/) (Table 2) as well as the measured particle number concentrations (Table 1).

The sampling system was located at the top floor (15 m above the ground) of Williams Hall in the main campus of Kent State University. Air was sampled at a fixed flow rate of 117 liters per minute (lpm) through an electrically grounded stainless steel stack (i.e. near-isokinetic) with a blower (Fantech company, model FX4). It is expected that the turbulent dispersion may cause nanoparticle loss within high flow manifold. For the inlet sampling flow rates (0.3 lpm, 0.6 lpm, or 1.0 lpm) used in this study, Reynolds number (*Re*) was varied between 70 and 392 (hence laminar flow). The inlet was installed to the backside of the building to avoid direct influence from the main parking lot. The closest highway (Interstate 76) is at the south and about 6.5 km away from the sampling site.

Three-day hourly air mass backward trajectories, arriving at 100 m above the ground level at the measurement site between 10 AM and 2 PM, were calculated with the National Oceanic and Atmospheric Administration (NOAA) Air Resources Laboratory (ARL) HYbrid Single-Particle Lagrangian Integrated Trajectory (HYSPLIT) PC version model (Draxler and Rolph, 2010) and using gridded wind fields from the Eta Data Assimilation System (EDAS) (Kanamitsu, 1989). We have also used HYSPLIT calculations to retrieve solar radiation data at the measurement site over a period of 4 years. Air masses were classified into five different categories according to their origin (Figs. 1 and 8): north, east, south, west, and slow moving local air masses. Air masses that spent at least a few days within an area of 200 km around the sampling site were referred to as slow moving air masses. A large number of coal-burning power plants are located to the east–southeast within 300 km. These major power plants include Keystone, Muskingum River, WH Sammis, and Conesville, with the SO_2 emissions greater than 10^5 tons/year (http://www.epa.gov/airdata/).

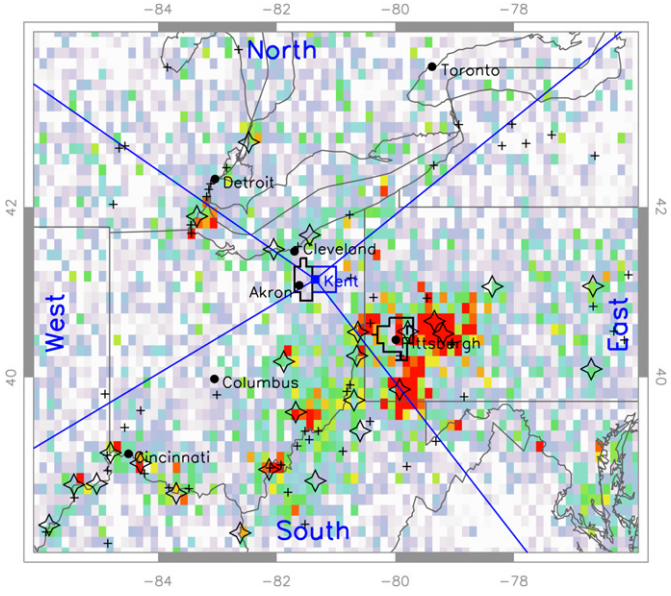

Fig. 1. A regional map showing a location of the sampling site, Kent (blue filled square) and surrounding urban areas (black dots). County boundaries for Kent (Portage), Akron (Summit) and Pittsburgh (Allegheny) are also shown (Table 2). The coal-burning power plant facilities with yearly SO_2 emissions $>3 \times 10^4$ tons (open stars) and SO_2 mass $<3 \times 10^4$ tons (plus signs) from 2006 to 2009 are also shown (from US Environmental Protection Agency Office of Air and Radiation under Acid Rain Program; http://www.epa.gov/air/data/geosel.html). Color in the background shows averaged OMI retrieved PBL SO_2 column amounts (in Dobson Units) over a 4-year time period from 2006 to 2009. High SO_2 concentrations (red color) are co-located with locations of major power plant facilities (open star). Air masses were grouped based on their origin, roughly divided by the blue lines. [For interpretation of the references to colour in this figure legend, the reader is referred to the web version of this article.]

Table 2
Emissions of air pollutants (SO_2, NO_x, CO, $PM_{2.5}$) in three counties for the year 2008 (http://www.epa.gov/).

Pollutant (10^3 tons)	Kent (Portage County) (161,419 inhabitants)	Akron (Summit County) (542,899 inhabitants)	Pittsburgh (Allegheny County) (1,223,348 inhabitants)
SO_2	0.3	5.3	49.8
NO_x	5.7	14.9	52.4
CO	42.1	126.2	260.3
$PM_{2.5}$	1.3	2.5	8.3

Meteorological data, including temperature and relative humidity (RH), at Akron-Canton regional airport weather station (about 30 km to the south of the sampling site), from US National Climatic Data Center (http://lwf.ncdc.noaa.gov/oa/ncdc.html), were also used in the analysis to examine meteorological influence on NPF. The fully automated "HO-83" hygrothermometer was used to measure the ambient temperatures and the dew point temperatures. It measures ambient temperature in the range of −50 °C to 50 °C, with a root mean square error of 0.5 °C and a resolution of 0.05 °C. The relative humidity was then calculated from the 5-min averages of ambient temperature and dew point temperature (ASOS, 1998). SO_2 and NO_x daily averaged data at the same weather station (http://www.epa.gov/airdata/) were also used to see the effects of power plant plumes. SO_2 was measured with a pulsed UV-fluorescence analyzer (Thermo Environmental, 43C-TLE); the detection limit was 0.05 ppbv with an uncertainty of ±10%. NO_x was measured with an ultra-sensitive chemiluminescence analyzer (Teledyne, model 200EU), with detection limit of 0.05 ppbv (http://www.epa.gov/).

In addition, ozone monitoring instrument (OMI) planetary boundary layer (PBL) SO_2 column data averaged over 2006–2009 was also used to co-locate point sources near Kent (Fig. 1). The OMI instrument, onboard NASA's Aura spacecraft in July 2004, retrieves PBL SO_2 column amounts from measurements of back-scattered solar UV radiation in the wavelength range from 310.8 to 314.4 nm, using a band residual difference algorithm (Krotkov et al., 2006). We have used Level 2 retrieved PBL SO_2 column data from the OMI. Daily gridded retrievals on 0.125° × 0.125° were first used to filter the data with relatively high cloud fraction (>0.2) and large solar zenith angle (>70°), and possible contamination due to the OMI row anomaly, and then averaged over 0.25° × 0.25° resolution.

2.2. Particle measurements and data reduction

Four-year measurements were performed using three sets of scanning mobility particle sizers (SMPS), comprising a nano differential mobility analyzer (NDMA, TSI 3085) with water condensation particle counter (CPC, TSI 3786), an NDMA (TSI 3085) with a butanol CPC (TSI 3776), and a long differential mobility analyzer (LDMA, TSI 3081) with a butanol CPC (TSI 3772). These three SMPS systems together can provide particle size range from 3 to 1000 nm. However, during 2008–2009, the LDMA (TSI 3081) was set to measure particle sizes from 13 to 611 nm and so for the consistency, we considered particles of diameter from 3 to 600 nm in the present study. This size range did not affect our conclusion, because the particle number concentrations and the condensational sink (*CS*) derived from particle sizes of 3–1000 nm were only 4% and 8% higher than those derived from particle sizes of 3–600 nm, respectively.

When measuring ultrafine particles, diffusion losses in the sampling line must be taken into account. With a fixed sampling tube length and a sample flow rate, particle losses due to diffusion increases with the decreasing particle size. We have corrected these size-dependent diffusional losses for the sampling line using empirical functions given by Baron and Willeke (2001). The particle

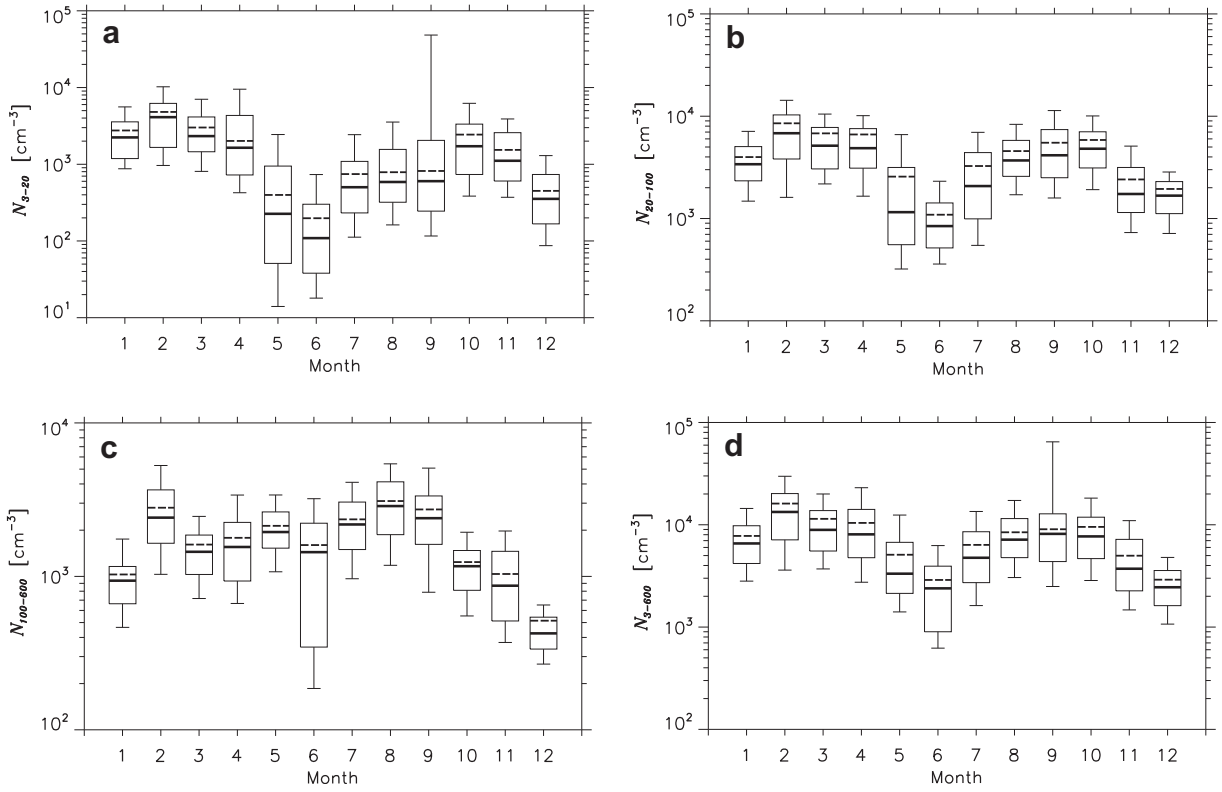

Fig. 2. Statistical analysis of nuclei mode (a), Aitken mode (b), accumulation mode (c), and total particle number (d) concentrations measured at Kent from 2006 to 2009. The median (horizontal solid lines), the mean (horizontal dotted lines), the 75th and 25th percentile (boxes), and the 90th and 10th percentile (whiskers) are shown.

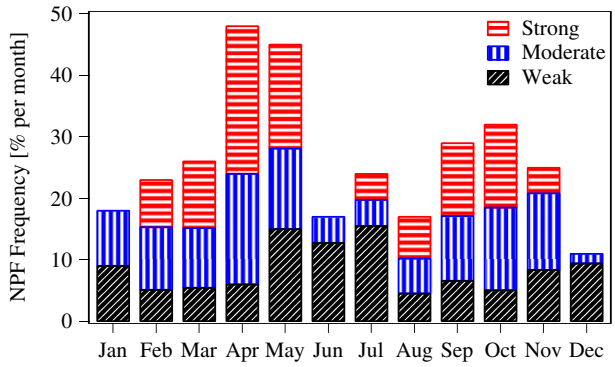

Fig. 3. The monthly mean frequency of different types of NPF events (strong, moderate, and weak) measured at Kent from 2006 to 2009.

fraction that penetrates the aerosols (P) in a circular tube of length, L, at a flow rate, Q, and for particles with a diffusion coefficient of D can be derived as function of the parameter $\mu = \pi DL/Q$ (Gormley and Kennedy, 1949). The penetrating fraction, P, is then calculated for the entire range of μ from the following equations:

$$P = 0.819\cdot e^{(-3.657\mu)} + 0.098\cdot e^{(-22.305\mu)} + 0.033\cdot e^{(-56.961\mu)} + 0.015\cdot e^{(-107.62\mu)}, \quad \text{for } \mu > 0.02 \tag{1}$$

$$P = 1.0 - 2.564\cdot\mu^{(2/3)} + 12\mu + 0.177\cdot\mu^{(3/4)}, \quad \text{for } \mu = 0.02 \tag{2}$$

Typically, a tube length of 35 cm with a diameter of 0.54 cm was used at inlet sampling flow rates of 0.3 lpm, 0.6 lpm, or 1.0 lpm. Under these conditions, the diffusion correction factor was about 28–48% and 3–6% for 3 nm and 20 nm size particles, respectively.

Particle size distributions were then checked to remove sporadic noises, based on total number concentrations (N_i) and the relative standard deviation (SD_i) in each size bin (i). If the N_i and SD_i less than 2.5th and greater than 97.5th percentile values of all N_i and SD_i, then the individual particle size distribution was removed. Particle number concentrations in four different size ranges: nuclei (3–20 nm, N_{3-20}), Aitken (20–100 nm, N_{20-100}), accumulation (100–600 nm, $N_{100-600}$), and total particles (3–600 nm, N_{3-600}) were then calculated. Condensational sink, CS, was calculated from the measured aerosol size distributions form 3–600 nm (CS_{3-600}). CS is a rate at which H_2SO_4 vapor condenses on pre-existing particles and hence is proportional to the surface area of total aerosol particles. A detailed calculation procedure for CS can be found elsewhere (Erupe et al., 2010; Kulmala et al., 2001a).

2.3. Inversion model to calculate nucleation and growth rates

PARrticle Growth And Nucleation (PARGAN) model has been used to calculate the particle nucleation rates (J) and growth rates (GR) from the measured aerosol size distributions. PARGAN was originally developed by Verheggen and Mozurkewich (2006) and has also been used for ambient observations (Erupe et al., 2010). PARGAN calculates GR (GR_{pargan}) and J (J_{pargan}) from the measured particle size distributions with inversion, by assuming that consecutive measurements at the same location are representative of the same air mass history. The particle growth rate is determined by non-linear regression analysis of the General Dynamic Equation (GDE) (Friedlander, 2000), to fit the measured change in particle size distribution over time. PARGAN model takes into account aerosol microphysical dynamics, including condensation, coagulation, deposition, and dilution. The time of formation of critical cluster (diameter of 1 nm) for the measured particles of a certain size was then evaluated from the calculated growth rates. Nucleation rate is then obtained by integrating the particle losses from the time of measurement to the time of nucleation. The PARGAN model provides a great deal of variability in the growth rate obtained over each individual measurement time interval (e.g. 5 min). It can be used to derive empirically based nucleation rates in a variety of situations (laboratory and atmospheric studies) (Verheggen and Mozurkewich, 2006).

In the present study, we have further improved PARGAN code to perform data analysis for the ambient data. We have used a simple method to smooth particle size distribution for the data which are clearly have NPF features, indicated by the typical noontime "banana" shaped aerosol size growth, but they are too noisy so that the original PARGAN code could not read them or produced unexpected growth rates due to large deviation in fitting parameters. First, we smoothed particle size distribution (smoothing width = 4) and fitted lognormal distribution to the smoothed particle size distribution. We have then used the fitted particle size distributions to derive particle growth rates and nucleation rates. This allowed us to analyze ~30% more ambient data than the previous PARGAN code. This is because the strong dependence of growth rate on the relative change in total particle number concentrations over time can lead to over-or under-estimation of

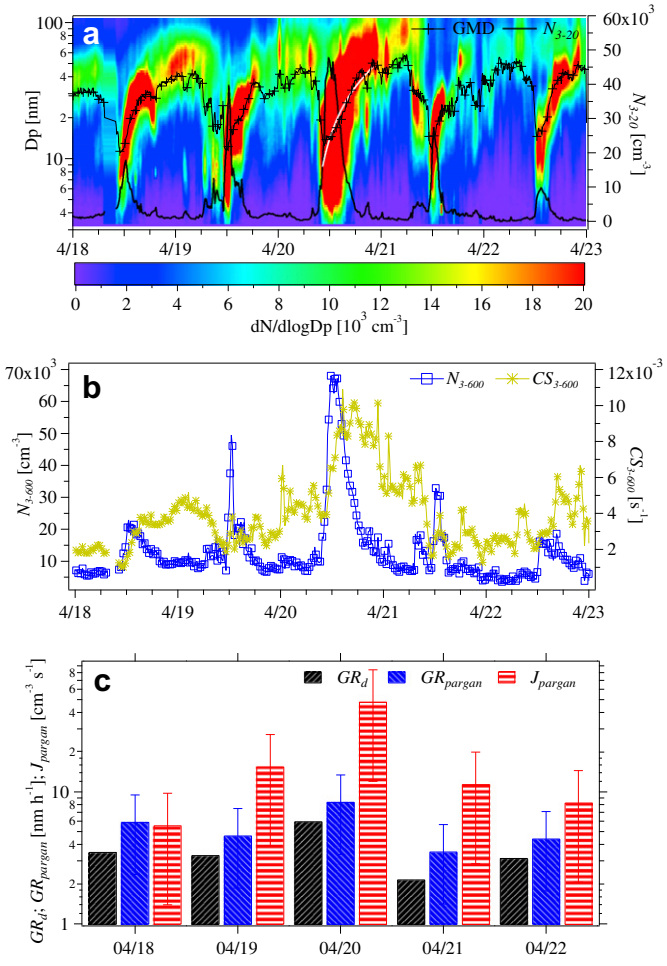

Fig. 4. Measurements from April 18–23, 2006. (a) Contour plot of typical particle size distributions. The N_{3-20} concentrations (solid white line) and the particle geometric mean diameter (black line with plus signs) are shown. (b) Time evolution of N_{3-600} (blue line with empty squares) and CS_{3-600} (yellow line with stars). (c) The GR_d (black), GR_{pargan} (blue) and J_{pargan} (red) for these NPF events. One standard deviation values for GR_{pargan} and J_{pargan} are shown with vertical bars. [For interpretation of the references to colour in this figure legend, the reader is referred to the web version of this article.]

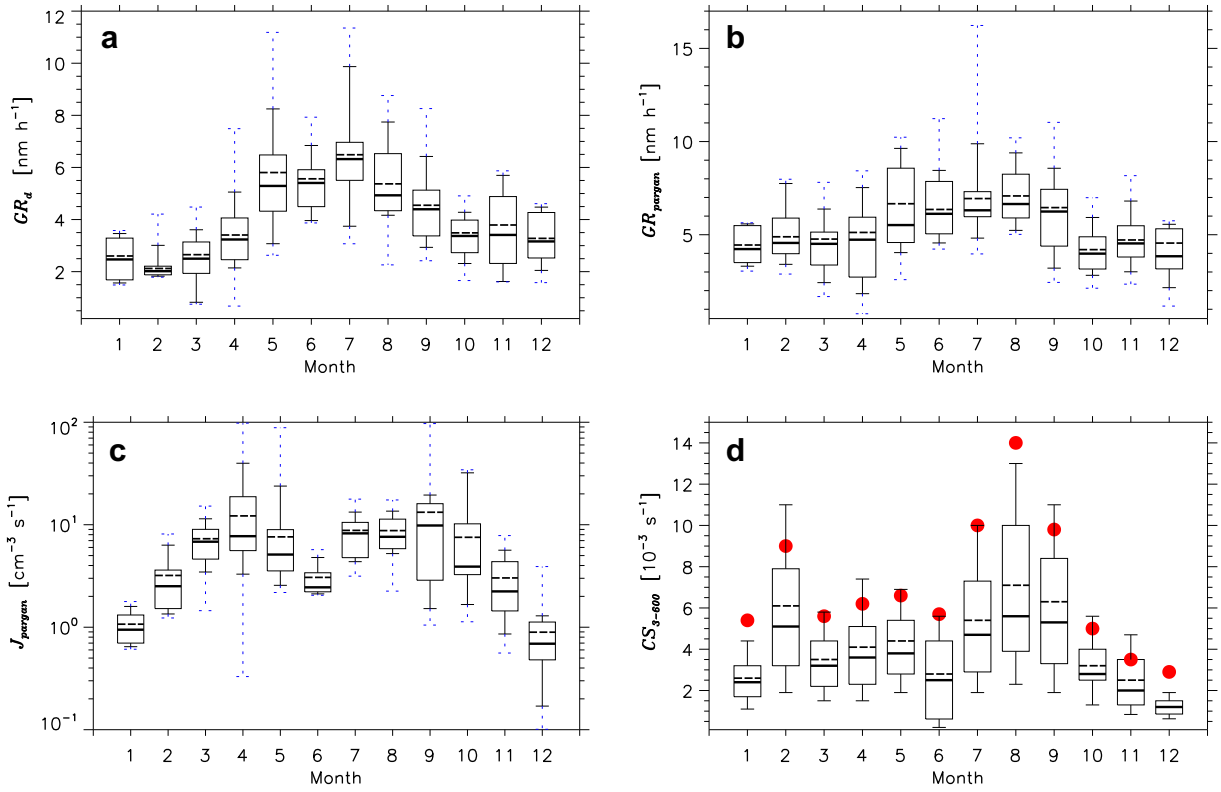

Fig. 5. The monthly variation of GR_d (a), GR_{pargan} (b), J_{pargan} (c), and CS_{3-600} (d) for all NPF for all NPF events observed from 2006 to 2009. The median (horizontal solid lines), mean (horizontal dotted lines), the 75th and 25th percentile (boxes), the 90th and 10th percentile (solid whiskers), and the minimum and maximum (dotted blue whiskers) are shown. The red filled circles shown in (d) indicate the median values of CS_{3-600} for the non-NPF event days, in comparison. [For interpretation of the references to colour in this figure legend, the reader is referred to the web version of this article.]

the growth rate, when the fitting parameters are either too large or too small.

Additionally, we have fitted a first-order polynomial line through geometric mean diameter to derive growth rates (GR_d). This approach was also previously reported by many researchers (Dal Maso et al., 2005; Erupe et al., 2010; Salma et al., 2005; Sihto et al., 2006).

3. Results and discussion

The total particle number concentrations in the size range from 3 to 600 nm measured at Kent were $(6.9 \pm 3.9) \times 10^3$ cm^{-3} (median and one standard deviation), within the range observed at other rural to semi-rural locations, $(2-11) \times 10^3$ cm^{-3} (Kivekaas et al., 2009; Pryor et al., 2010) and lower than that in urban locations such as Pittsburgh, 22×10^3 cm^{-3} (Stanier et al., 2004a) and Leipzig, Germany, 21.4×10^3 cm^{-3} (Wehner and Wiedensohler, 2003). Fig. 2 shows the monthly variation of particle number concentrations of nuclei mode, Aitken mode, accumulation mode, and total particles. The number concentration of nuclei mode, Aitken mode and total particles showed a clear monthly variation, higher during the spring and fall ($\sim 10 \times 10^3$ cm^{-3}) than in the summer and winter ($<10^3$ cm^{-3}). The accumulation mode particle number concentrations were highest during the summer and lowest in the winter.

We classified aerosol size distributions into four categories based on the growth of the measured nuclei mode concentrations: $dN_{3-20}/dt \leq 2000$ cm^{-3} h^{-1} as a non-NPF or unidentified event, $2000 \leq dN_{3-20}/dt < 4000$ cm^{-3} h^{-1} as a weak event, $4000 \leq dN_{3-20}/dt < 15{,}000$ cm^{-3} h^{-1} as a moderate event, and $N_{3-20} \geq 15{,}000$ cm^{-3} h^{-1} as a strong event. There were occasionally some sporadic occurrences of nuclei mode particles, which were difficult to identify as an NPF or non-NPF event, but since such cases were rare, we have grouped the non-NPF and unidentified events together. Short-lived events with elevated particle concentrations during traffic hours may be important in urban areas (Stanier et al., 2004b), but those traffic-related events were very rare at our semi-rural site. We have analyzed four years of data (2006–2009) comprising 587 days of observations, and found 191 NPF events (i.e. 33% of all observation days) and 396 non-NPF events (67%; including unidentified event days).

Fig. 3 illustrates the monthly variation of NPF occurrences. The number of NPF events were highest during the spring (March–May) with 80 events (41% of the total NPF events observed over the year), followed by 53 events (28%) in the fall (September–November), 36 events (18%) in the summer (June–August), and 22 events (12%) in the winter (December–February). This seasonal trend of NPF frequency was consistent with those found in other environmental locations, including urban (Stanier et al., 2004a), rural (Birmili et al., 2003), semi-rural (Pryor et al., 2010), and remote (Dal Maso et al., 2005; Kulmala et al., 2001b). While atmospheric observations in general have shown the highest NPF frequency in the spring and fall, there are also some exceptions in other locations. For example, NPF measurements in the rural Ispra region of Po Valley showed that the NPF frequency was higher during the fall (Rodriguez et al., 2005). In the rural St. Louis, the NPF frequency was lowest during the winter, with no clear seasonal trend in other seasons (Kulmala et al., 2004).

Fig. 4 shows the typical consecutive 5-day NPF events observed during the spring. For these events, particle size distributions displayed a burst of small particles and a sustained growth in the size and in N_{3-20} concentrations, $(8-45) \times 10^3$ cm^{-3}. The total particle number concentrations also increased abruptly during NPF events. The CS_{3-600} appears to be decreasing, likely due to dilution, prior to

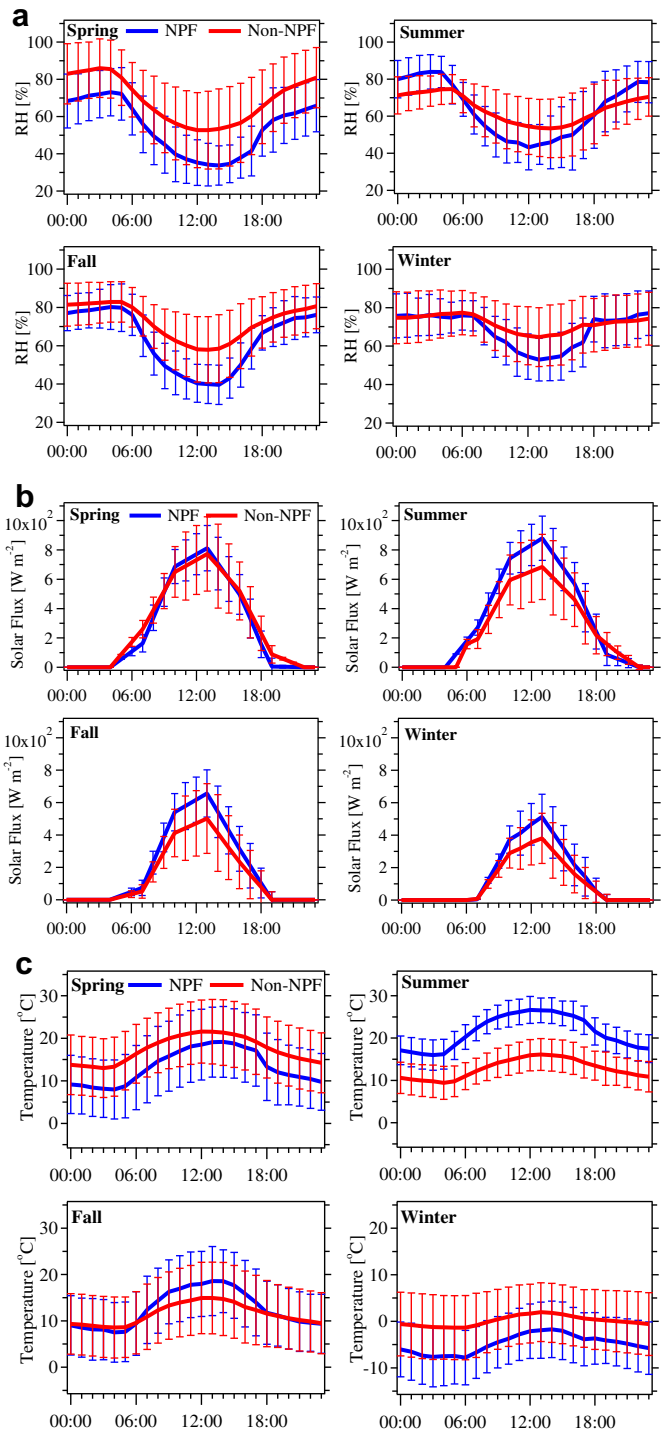

Fig. 6. The diurnal variation of the average relative humidity (a) solar flux (b) and temperature (c) on event and non-event days over entire study period.

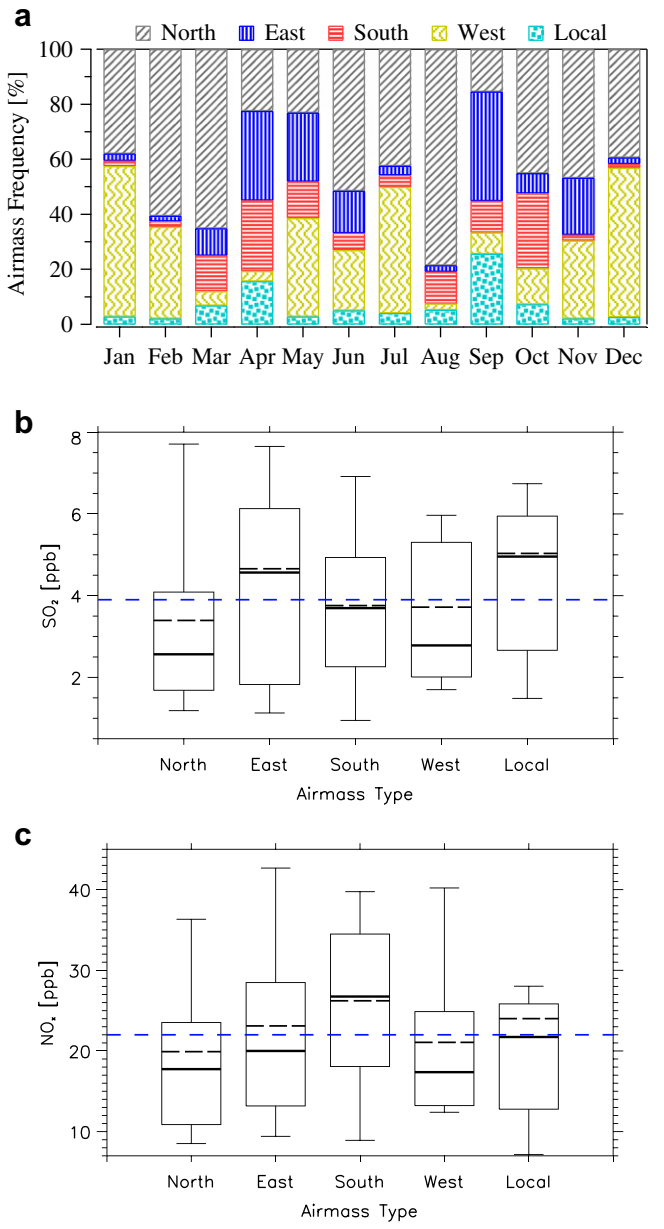

Fig. 7. (a) The monthly statistics of air masses of the observed NPF event days during 2006– 2009. The seasonal variation of SO_2 (b) and NO_x (c) as function of air masses for the NPF event days. The median (horizontal solid lines), mean (horizontal dotted lines), the 75th and 25th percentile (boxes), and the 90th and 10th percentile (solid whiskers) are shown.

the onset of nucleation, followed by an increase in CS_{3-600}, appearing a maximum during the night. Particle nucleation occurred just after a sufficient reduction in the particle surface area and then the small particles grew to larger sizes (~80 nm). The calculated particle growth rates (GR_{pargan}) (2.0–8.0 nm h^{-1}) were comparable to GR_d derived from particle geometric mean diameters (1.5–6.0 nm h^{-1}). The particle nucleation rates (J_{pargan}) for these events ranged from 5 to 48 cm^{-3} s^{-1}, with a median value of 11 ± 17 cm^{-3} s^{-1}.

Fig. 5 shows the median values of GR_d, GR_{pargan} and J_{pargan} for 167 NPF events, out of the total 191 events observed over a 4-year period. For the remaining 24 event days, PARGAN was not able to run because the data were still too noisy or sporadic even after smoothing. The derived GR_d ranged from 0.5 to 12 nm h^{-1}, with a median value of 3.9 ± 1.4 nm h^{-1}. The GR_{pargan} varied from 0.5 to 17 nm h^{-1}, with a median value of 5.1 ± 1.0 nm h^{-1}. These growth rates measured at our site were within the range of those observed at many other locations (0.1–17 nm h^{-1}) (Birmili et al., 2003; Dal Maso et al., 2005; Kulmala et al., 2005; Mäkelä et al., 2000; Pryor et al., 2010; Salma et al., 2005). The growth rates were also found highest during the summer (~6.5 nm h^{-1}) than in other seasons (~4.6 nm h^{-1}) (Fig. 5); this may be because there are higher concentrations of condensable species generated from oxidation

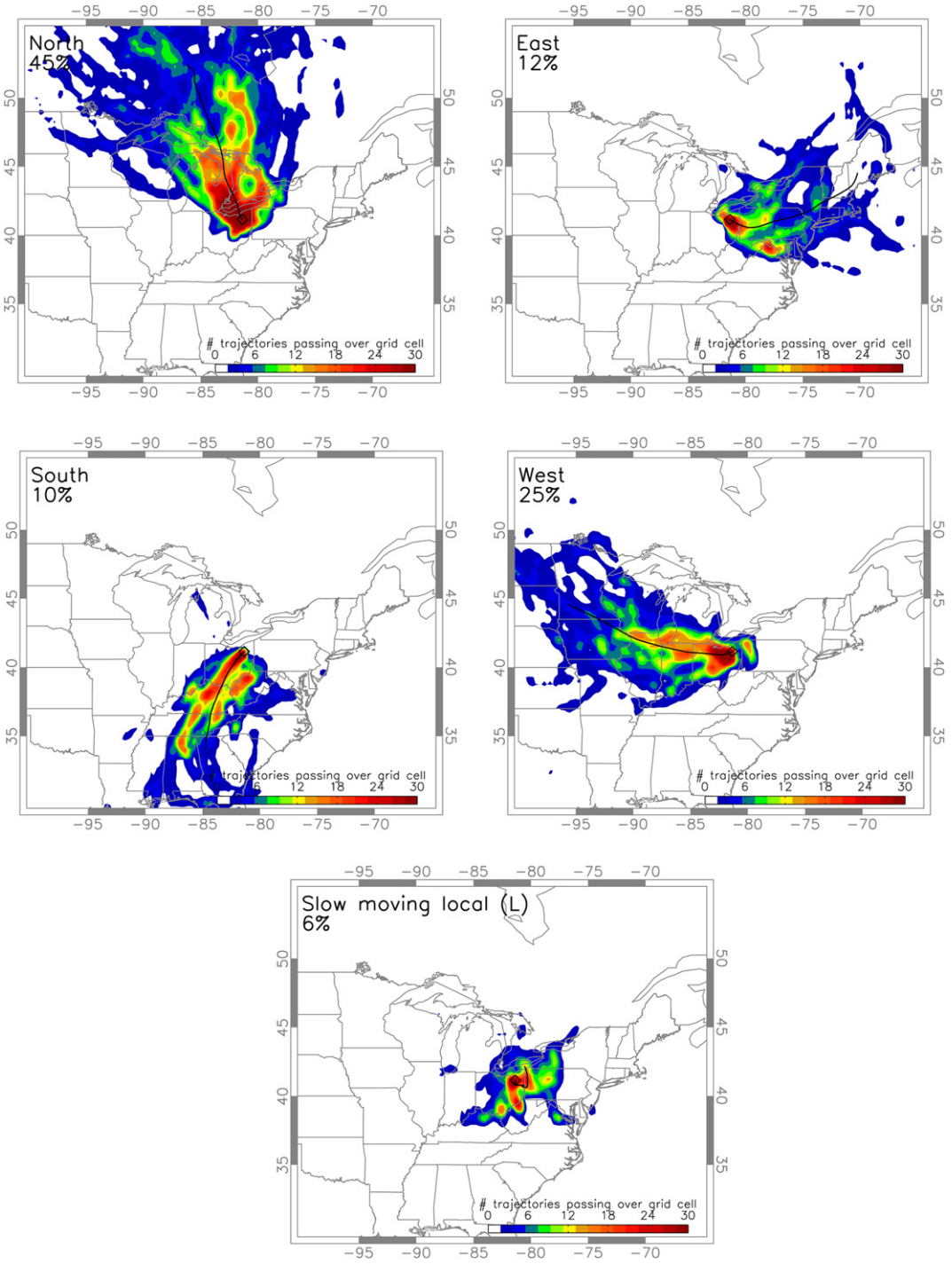

Fig. 8. Maps of three-day HYSPLIT back trajectories arriving at 100 m above ground between 10 AM and 2 PM local time at the measurement site, on observed NPF event days during 2006–09. The mean air mass trajectory (thick black line) and cluster frequency (%) for each cluster is also shown.

reactions of volatile organic compounds with hydroxyl radicals and ozone, leading to large growth rates. This seasonal behavior is similar to that found in other locations (Dal Maso et al., 2005; Salma et al., 2005), which also derived growth rates from the slope of first-order polynomial fitting to the aerosol sizes. A relatively good correlation between GR_d and GR_{pargan} was also found ($R^2 = 0.6$).

J_{pargan} varied from 0.1 to 100 cm^{-3} s^{-1}, with a median value of 4.8 ± 3.1 cm^{-3} s^{-1}. This value lies within the range (0.01–10 cm^{-3} s^{-1}) found in regional nucleation events in the continental boundary layer (Kulmala et al., 2004). The annual variation pattern showed higher J_{pargan} in the spring and fall than in the summer and winter, analogous to observed NPF frequency (Fig. 3). In the spring and fall, the particle nucleation rates were occasionally observed as high as 100 cm^{-3} s^{-1}, which could be linked to the transported industrial plumes, containing intense SO_2 (as will be discussed later in this section). This seasonal variation is inline with previous observations at mid-latitude locations (Dal Maso et al., 2005; Mäkelä et al., 2000). An important feature is that J_{pargan} was not directly correlated to GR_d or GR_{pargan}

(Fig. 5), implying that different chemical species are required for particle nucleation and growth processes.

The seasonal variation of CS_{3-600} showed a maximum in the summer (Fig. 5), consistent with higher concentrations of accumulation mode particles (Fig. 2). The CS_{3-600} over NPF event days [$(3.6 \pm 1.5) \times 10^{-3}$ s^{-1}] was lower than during non-NPF days [$(6.0 \pm 4.2) \times 10^{-3}$ s^{-1}]. In general, atmospheric observations showed that NPF is often associated with low CS_{3-600} (Dal Maso et al., 2005; Kulmala et al., 2001b; Salma et al., 2005), but NPF was also observed in polluted areas at high CS_{3-600} when H_2SO_4 concentrations were high enough (Fiedler et al., 2005).

In addition to CS_{3-600}, other factors, such as RH, solar radiation, temperature, and air mass history, can also affect NPF. The average diurnal variations of RH for NPF and non-NPF events are shown in Fig. 6a. The RH was generally lower on the event days compared to the non-event days during all seasons. During the noontime, the average RH was lowest in the spring (~33%), followed by the fall (~37%), summer (~44%) and winter (~52%), analogous to the observed seasonal trend of NPF frequency (Fig. 3). Our analysis thus suggests that NPF may be anti-correlated with RH, consistent with previous reports at different continental locations (Birmili et al., 2003; Stanier et al., 2004b). In order to statistically test the anti-correlation between RH and NPF frequency, a Mann–Whitney–Wilcoxon *U*-test was performed and a statistically highly significant difference ($p < 0.005$) was found. It is possible that at a higher RH, hygroscopic growth of aerosol particles may produce higher *CS* (Hamed et al., 2011). Indeed, the CS_{3-600} was highest in the summer (Fig. 5) and this may explain the low NPF frequency seen in the summer. Solar radiation is also an important parameter in the initial step of atmospheric nucleation, since formation of condensable species via photochemical reactions is required for nucleation. In all seasons, the solar radiation was higher on NPF event days than non-event days (Fig. 6b). The temperatures showed a larger difference between the nighttime minimum and the daytime maximum on event days, compared to non-event days (Fig. 6c), as observed at other location (Birmili et al., 2003). Based on a Mann–Whitney–Wilcoxon *U*-test for solar radiation and temperature, the differences were also statistically significant, $p < 0.0005$ and $p < 0.05$, respectively. Additionally, the differences between solar radiation minimum/maximum on NPF and non-NPF event days were also statistically highly significant ($p < 10^{-5}/p < 10^{-15}$).

NPF processes are shown to be strongly dependent on meteorological conditions of air masses (Kulmala et al., 2004; Nilsson et al., 2001). From our analysis, it appears that the high NPF frequency seen in the spring and fall was often related to air masses affected by anthropogenic plumes from industrial sectors (such as coal-burning power plants) at the east–southeast of the measurement site (Fig. 1). Polluted air masses (east, south, and local) were more frequent in spring and fall (~10–20%) compared to summer and winter (~1–5%) (Fig. 7a). The mean SO_2 and NO_x concentrations associated with the polluted air masses were also higher (Fig. 7b and c). Based on a Mann–Whitney–Wilcoxon *U*-test for SO_2 and NO_x emission between the sectors, e.g. North (relatively clean) and East (polluted), the statistically significant differences were observed ($p < 0.05$). A very good correlation between SO_2 and NO_x concentrations ($R^2 = 0.7$) was indicative of the plume of anthropogenic origin. Although SO_2 and NO_x data were taken from the weather station located about 30 km to the south of the measurement site, both the locations had relatively similar emissions of trace gases and particulate matter (PM 2.5) compared to other urban areas to the south–southeast of the measurement site (Table 2).

Studies from semi-rural site in the Midwestern USA (Indiana) have also observed frequent NPF events under the influence of intense sulfur plumes from polluted areas, containing high concentrations of H_2SO_4 (in the 10^7–10^8 range) and SO_2 (Pryor et al., 2011, 2010). Additionally, these two locations showed similar seasonal trend of NPF frequency and particle growth rates. On the other hand, NPF occurred more frequently during the spring season at the Indiana site (~46%) compared to that of our measurement site (~30%). The other differences include *CS*, which was higher (5×10^{-3}–5×10^{-2} s^{-1}) at Indiana site, possibly due to its closer proximity to large urban areas, than at our measurement site [$(3.6 \pm 1.5) \times 10^{-3}$ s^{-1}].

4. Conclusions

We have analyzed the seasonal variation of NPF characteristics using the 4-year measurements of particle size distributions between 3 and 600 nm in a semi-rural continental environment of the United States. The NPF frequency was highest in the spring (~40%) and minimum in winter (~17%). The nucleation rates were also highest in spring (6.8 ± 1.3 cm^{-3} s^{-1}) and lowest in winter (1.0 ± 0.9 cm^{-3} s^{-1}), showing the same seasonal trend as the NPF frequency. The growth rates were highest in summer (6.4 ± 0.4 nm h^{-1}) and lowest in winter (4.2 ± 0.3 nm h^{-1}). The particle nucleation rates and growth rates showed different seasonal trends, suggesting that the different species may be involved in particle nucleation and growth processes. The nuclei and Aitken mode particle concentrations were highest in the spring and fall and lowest in the summer and winter, related to the higher nucleation rates in the spring and fall, whereas the accumulation mode particle concentrations were highest in the summer, linked to higher growth rates in the summer. The high NPF frequency during the spring and fall seemed to be associated with polluted air masses arriving from the east–southeast, containing higher SO_2 concentrations. In general, NPF events were associated with lower RH, lower *CS*, and higher solar radiation.

Acknowledgments

We thank funding support from NSF (AGS-1137821; CAREER ATM-0645567), NOAA (NA08OAR4310537), and Ohio Board Regents; and Li-Hao Young, Mark Erupe and Huan Yu for technical assistances and useful discussions. We also thank NASA Goddard Earth Sciences Data and Information Services Center for providing OMI retrieved SO_2 data, U.S. EPA office of Air and Radiation for providing trace gases and meteorological data from Akron-Canton airport monitoring site, and NOAA ARL for providing HYSPLIT air-mass back trajectory calculations.

Appendix A. Supplementary material

Supplementary data related to this article can be found online at http://dx.doi.org/10.1016/j.atmosenv.2012.05.047.

References

ASOS, 1998. Automated Surface Observing System (ASOS) – User's Guide. http://www.nws.noaa.gov/asos/.

Baron, P.A., Willeke, K., 2001. Aerosol Measurement: Principles, Techniques, and Applications, second ed. John Wiley and Sons, New York.

Birmili, W.H., Berresheim, H., Plass-Dulmer, C., Elste, T., Gilge, S., Wiedensohler, A., Uhrner, U., 2003. The Hohenpeissenberg aerosol formation experiments (HAFEX): a long-term study including size-resolved aerosol, H_2SO_4, OH, and monoterpenes measurements. Atmos. Chem. Phys. 3, 361–376.

Clarke, A.D., 1992. Atmospheric nuclei in the remote free-troposphere. J. Atmos. Chem. 14, 479–488.

Dal Maso, M., Kulmala, M., Riipinen, I., Wagner, R., Hussein, T., Aalto, P., Lehtinen, E.J., 2005. Formation and growth rates of fresh atmospheric aerosols: eight years of aerosol size distribution data from SMEARII, Hyytiälä, Finland. Boreal Environ. Res. 10, 323–336.

Draxler, R.R., Rolph, G.D., 2010. HYSPLIT (HYbrid Single-particle Lagrangian Integrated Trajectory) Model. NOAA ARL READY website:. NOAA Air Resources Laboratory, Silver Spring, MD http://ready.arl.noaa.gov/HYSPLIT.php.

Erupe, M.E., Benson, D.R., Li, J., Young, L.-H., Verheggen, B., Al-Refai, M., Tahboub, O., Cunningham, V., Frimpong, F., Viggiano, A.A., Lee, S.-H., 2010. Correlation of aerosol nucleation rate with sulfuric acid and ammonia in Kent Ohio: an atmospheric observation. J. Geophys. Res. 115, D23216.

Fiedler, V., Dal Maso, M., Boy, M., Aufmhoff, H., Hoffmann, J., Schuck, T., Birmili, W., Hanke, M., Uecker, J., Arnold, F., Kulmala, M., 2005. The contribution of sulphuric acid to atmospheric particle formation and growth: a comparison between boundary layers in Northern and Central Europe. Atmos. Chem. Phys. 5, 1773–1785.

Friedlander, S.K., 2000. Smoke Dust and Haze. Oxford University Press, Oxford.

Gormley, P.G., Kennedy, M., 1949. Diffusion from a stream flowing through a cylindrical tube. Proc. R. Ir. Acad. A52, 163–169.

Hallar, A.G., Lowenthal, D.H., Chirokova, G., Borys, R.D., Wiedinmyer, C., 2011. Persistent daily new particle formation at a mountain-top location. Atmos. Environ. 45, 4111–4115.

Hamed, A., Korhonen, H., Sihto, S.-L., Joutsensaari, J., Jarvinen, H., Petaja, T., Arnold, F., Nieminen, T., Kulmala, M., Smith, J.N., Lehtinen, K.E.J., Laaksonen, A., 2011. The role of relative humidity in continental new particle formation. J. Geophys. Res. 116, D03202.

Kanamitsu, M., 1989. Description of the NMC global data assimilation and forecast system. Weather Forecast 4, 335–342.

Kivekaas, N., Sun, J., Zhan, M., Kerminen, V.-M., Hyvarinen, A.-P., Komppula, M., Viisanen, Y., Hong, N., Zhang, Y., Kulmala, M., Zhang, X.-C., Deli-Geer, Lihavainen, H., 2009. Long term particle size distribution measurements at Mount Waliguan, a high altitude site in inland China. Atmos. Chem. Phys. 9, 5461–5474.

Krotkov, N.A., Carn, S.A., Krueger, A.J., Bhartia, P.K., Y K, 2006. Band residual difference algorithm for retrieval of SO_2 from the Aura Ozone Monitoring Instrument (OMI). IEEE Trans. Geosci. Remote Sens. 44, 1259–1266.

Kuang, C., McMurry, P.H., McCormick, A.V., Eisele, F.L., 2008. Dependence of nucleation rates on sulfuric acid vapor concentration in diverse atmospheric locations. J. Geophys. Res. 113, D10209.

Kulmala, M., dal Maso, M., Makela, J.M., Pirjola, L., Vakeva, M., Aalto, P., Miikkulainen, P., Hameri, K., O'Dowd, C.D., 2001a. On the formation, growth, and composition of nucleation mode particles. Tellus 53B, 479–490.

Kulmala, M., Hämeri, K., Aalto, P.P., Mäkelä, J.M., Pirjola, L., Nilsson, E.D., Buzorius, G., Rannik, U., D.M., M., Seidl, W., Hoffman, T., Janson, R., Hansson, H.C., Viisanen, Y., Laaksonen, A., O'Dowd, C.D., 2001b. Overview of the international project on biogenic aerosol formation in the boreal forest (BIOFOR). Tellus 53, 324–343.

Kulmala, M., Petäjä, T., Mönkkönen, P., Koponen, I.K., Dal Maso, M., Aalto, P.P., Lehtinen, K.E.J., Kerminen, V.-M., 2005. On the growth of nucleation mode particles: source rates of condensable vapor in polluted and clean environments. Atmos. Chem. Phys. 5, 409–416.

Kulmala, M., Rannik, Ü., Pirjola, L., Dal Maso, M., Karimäki, J., Asmi, A., Jäppinen, A., Karhu, V., Korhonen, H., Malvikko, S.-P., Puustinen, A., Raittila, J., Romakkaniemi, S., Suni, T., Yli-Koivisto, S., Paatero, J., Hari, P., Vesala, T., 2000. Characterization of atmospheric trace gas and aerosol concentrations at forest sites in southern and northern Finland using back trajectories. Boreal Environ. Res. 5, 315–336.

Kulmala, M., Vehkamaki, H., Petaja, T., dal Maso, M., Lauri, A., Kerminen, V.M., Birmili, W.H., McMurry, P.H., 2004. Formation and growth rates of ultrafine atmospheric particles: a review of observations. J. Aerosol Sci. 35, 143–176.

Laakso, L., Hussein, T., Aarnio, P., Komppula, M., Hiltunen, V., Viisanen, Y., Kulmala, M., 2003. Diurnal and annual characteristics of particle mass and number concentrations in urban, rural and Arctic environments in Finland. Atmos. Environ. 37, 2629–2641.

Lee, S.-H., Reeves, J.M., Wilson, J.C., Hunton, D.E., Viggiano, A.A., Miller, T.M., Ballenthin, J.O., Lait, L.R., 2003. Particle formation by ion nucleation in the upper troposphere and lower stratosphere. Science 301, 1886–1889.

Lovejoy, E.R., Curtius, J., Froyd, K.D., 2004. Atmospheric ion-induced nucleation of sulfuric acid and water. J. Geophys. Res. 109, D08204.

Mäkelä, J.M., Dal Maso, M., Pirjola, L., Keronen, P., Laakso, L., Kulmala, M., Laaksonen, A., 2000. Characteristics of the atmospheric particle formation events observed at a boreal forest site in southern Finland. Boreal Environ. Res. 5, 299–313.

Marti, J.J., Weber, R.J., McMurry, P.H., Eisele, F., Tanner, D., Jefferson, A., 1997. New particle formation at a remote continental site: assessing the contributions of SO_2 and organic precursors. J. Geophys. Res. 102, 6331–6339.

McMurry, P.H., Fink, M., Sakuri, H., Stolzenburg, M., Mauldin III, R.L., Smith, J., Eisele, F.L., Moore, K., Sjostedt, S., Tanner, D., Huey, L.G., Nowak, J.B., Edgerton, E., Voisin, D., 2005. A criterion for new particle formation in the sulfur-rich Atlanta atmosphere. J. Geophys. Res. 110, D22S02.

Morawska, L., Jayarantne, E.R., Mengersen, K., Thomas, S., 2002. Differences in airborne particle and gaseous concentrations in urban air between weekdays and weekends. Atmos. Environ. 36, 4375–4383.

Nilsson, E.D., Paatero, J., Boy, M., 2001. Effects of air masses and synoptic weather on aerosol formation in the continental boundary layer. Tellus B 53, 462–478.

Pierce, J.R., Leaitch, W.R., Liggio, J., Westervelt, D.M., Wainwright, C.D., Abbatt, J.P.D., Ahlm, L., Al-Basheer, W., Cziczo, D.J., Hayden, K.L., Lee, A.K.Y., Li, S.-M., Russell, L.M., Sjostedt, S.J., Strawbridge, K.B., Travis, M., Vlasenko, A., Wentzell, J.J.B., Wiebe, H.A., Wong, J.P.S., Macdonald, A.M., 2012. Nucleation and condensational growth to CCN sizes during a sustained pristine biogenic SOA event in a forested mountain valley. Atmos. Chem. Phys. 12, 3147–3163.

Pryor, S.C., Barthelmie, R.J., Sørensen, L.L., McGrath, J.G., Hopke, P., Petaja, T., 2011. Spatial and vertical extent of nucleation events in the Midwestern USA: insights from the Nucleation in ForesTs (NIFTy) experiment. Atmos. Chem. Phys. 11, 1641–1657.

Pryor, S.C., Spaulding, A.M., Barthelmie, R.J., 2010. New particle formation in the Midwestern USA: event characteristics, meteorological context and vertical profiles. Atmos. Environ. 44, 4413–4425.

Rodriguez, S., Van Dingenen, R., Putaud, J.-P., Martins-Dos Santos, S., Roselli, D., 2005. Nucleation and growth of new particles in the rural atmosphere of Northern Italy – relationship to air quality monitoring. Atmos. Environ. 39, 6734–6746.

Salma, I., Borsós, T., Weidinger, T., Aalto, P., Hussein, T., Dal Maso, M., Kulmala, M., 2005. Production, growth and properties of ultrafine atmospheric aerosol particles in an urban environment. Atmos. Chem. Phys. 11, 1339–1353.

Sihto, S.-L., Kulmala, M., Kerminen, V.-M., Dal Maso, M., Petäjä, T., Riipinen, I., Korhonen, H., Arnold, F., Janson, R., Boy, M., Laaksonen, A., Lehtinen, K.E.J., 2006. Atmospheric sulfuric acid and aerosol formation: implications form atmospheric measurements for nucleation and early growth mechanisms. Atmos. Chem. Phys. 6, 4079–4091.

Smith, J.N., Dunn, M.J., VanReken, T.M., Iida, K., Stolzenburg, M.R., McMurry, P.H., Huey, L.G., 2008. Chemical composition of atmospheric nanoparticles formed from nucleation in Tecamac, Mexico: evidence for an important role for organic species in nanoparticle growth. Geophys. Res. Lett. 35, L04808.

Spracklen, D.V., Carslaw, K.S., Kulmala, M., Kerminen, V.-M., Sihto, S.-L., Riipinen, I., Merikanto, J., Mann, G.W., Chipperfield, M.P., Wiedensohler, A., Birmili, W., Lihavainen, H., 2008. Contribution of particle formation to global cloud condensation nuclei concentrations. Geophys. Res. Lett. 35, L06808.

Stanier, C.O., Khlystov, A.Y., Pandis, S.N., 2004a. Ambient aerosol size distributions and number concentrations measured during the Pittsburgh Air Quality Study (PAQS). Atmos. Environ. 38, 3275–3284.

Stanier, C.O., Kylstov, A.Y., Pandis, S.N., 2004b. Nucleation events during the Pittsburgh air quality study: description and relation to key meteorological, gas phase, and aerosol parameters. Aerosol Sci. Technol. 38, 253–264.

Tunved, P., Hansson, H.-C., Kulmala, M., Aalto, P., Viisanen, Y., Karlsson, H., Kristensson, A., Swietlicki, E., Dal Maso, M., Ström, J., Komppula, M., 2003. One year boundary layer aerosol size distribution data from five Nordic background stations. Atmos. Chem. Phys. 3, 2183–2205.

Verheggen, B., Mozurkewich, M., 2006. An inverse modeling procedure to determine particle growth and nucleation rates from measured aerosol size distributions. Atmos. Chem. Phys. 6, 2927–2942.

Weber, R.J., McMurry, P.H., Mauldin III, R.L., Tanner, D., Eisele, F.L., Clarke, A.D., Kapustin, V.N., 1999. New particle formation in the remote troposphere: a comparison of observations at various sites. Geophys. Res. Lett. 26, 307–310.

Wehner, B., Wiedensohler, A., 2003. Long term measurements of submicrometer urban aerosols: statistical analysis for correlations with meteorological conditions and trace gases. Atmos. Chem. Phys. 3, 867–879.